Tailoring the Electronic and Magnetic Properties of Two-Dimensional Silicon Carbide Sheets and Ribbons by Fluorination

Zhiming Shi,[†,§] Alex Kutana,[‡] Guangtao Yu,[†] Wei Chen,[†] Boris I. Yakobson,[‡] Udo Schwingenschlogl,[*,§] and Xuri Huang[*,†]

[†]Institute of Theoretical Chemistry, Jilin University, Changchun 130023, People's Republic of China

[‡]Department of Materials Science and NanoEngineering, Department of Chemistry, and the Smalley Institute for Nanoscale Science and Technology, Rice University, Houston, Texas 77005, United States

[§]King Abdullah University of Science and Technology (KAUST), Physical Science and Engineering Division (PSE), Thuwal 23955-6900, Saudi Arabia

Ⓢ *Supporting Information*

ABSTRACT: Fluorination has been instrumental for tuning the properties of several two-dimensional (2D) materials, including graphene, h-BN, and MoS_2. However, its potential application has not yet been explored in 2D silicon carbide (SiC), a promising material for nanoelectronic devices. We investigate the structural, electronic, and magnetic properties of fully and partially fluorinated 2D SiC sheets and nanoribbons by means of density functional theory combined with cluster expansion calculations. We find that fully fluorinated 2D SiC exhibits chair configurations and a nonmagnetic semiconducting behavior. Fluorination is shown to be an efficient approach for tuning the band gap. Four ground states of partially fluorinated SiC, $SiCF_{2x}$ with x = 0.0625, 0.25, 0.5, 0.75, are obtained by cluster expansion calculations. All of them exhibit nanoroad patterns, with the x = 0.5 structure identified as the most stable one. The x = 0.0625 structure is a nonmagnetic metal, while the other three are all ferromagnetic half-metals, whose properties are not affected by the edge states. We propose an effective approach for modulating the electronic and magnetic behavior of 2D SiC, paving the way to applications of SiC nanostructures in integrated multifunctional and spintronic nanodevices.
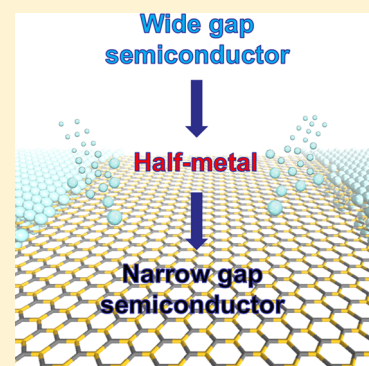
1. INTRODUCTION

Since graphene, the two-dimensional (2D) single atom thick hexagonal sheet of sp^2-hybridized C atoms, was first fabricated by Novoselov et al. in 2004,[1] many intriguing properties have been found to result from its long-range delocalized π-conjugation,[2,3] for example, massless Dirac fermions,[4] the highest carrier mobility,[5] and record mechanical strength.[6] Research therefore has been largely extended to other inorganic 2D materials. In recent years, numerous 2D materials have been reported, such as BN,[7] SiC,[8,9] CN,[10] ZnO,[11] and MS_2,[7,12] (M = Mo, W, Sn). Particularly, 2D SiC is widely expected to be useful in electronic devices because of the maturity of the silicon technology. SiC nanostructure polymorphs have been synthesized via several routes by several research groups.[13−15] Wu et al.[13] have reported the synthesis of bicrystalline SiC nanobelts via thermal evaporation and condensation with silicon powder and multiwall carbon nanotubes as raw materials at 1250 °C. SiC nanoribbons (NRs) that are tens to hundreds of micrometers long and several micrometers wide have been synthesized by a reaction of silicon vapor and carbon black powder at 1500 °C in Ar atmosphere at atmospheric pressure.[15] In addition, 3C-SiC nanobelts have been realized via lithium-assisted synthesis at a moderate temperature by Gao et al.[14] Theoretical investigations have revealed that monolayer SiC is a

nonmagnetic (NM) semiconductor[8] with high stability and in-plane stiffness,[16] which is ideal for nanoelectronic devices, in contrast to the large band gap of 2.53 eV.[8,16] Hence, tuning the electronic properties of 2D SiC can further broaden the range of possible applications. Semiconductors, metals, and half-metals can be realized through different approaches, for example, cutting NRs,[17,18] inducing defects,[19,20] applying external electrical fields,[21] doping foreign atoms,[22] and chemical covalent modification.[23−27]

Being an efficient approach toward surface functionalization, fluorination has been widely studied for tuning the magnetic and electronic properties of 2D materials experimentally and theoretically.[23,28−39] Until recently, fluorographene has attracted the most attention. In contrast to zero band gap semimetallic pristine graphene, fluorographene has been confirmed as a wide-gap semiconductor (3.0 eV).[29−32] Partially fluorinated graphene also has been synthesized in recent works.[29,30] For instance, C_4F with 25% coverage of F atoms adsorbed on one side of graphene has been produced and density functional theory calculations have resulted in a band
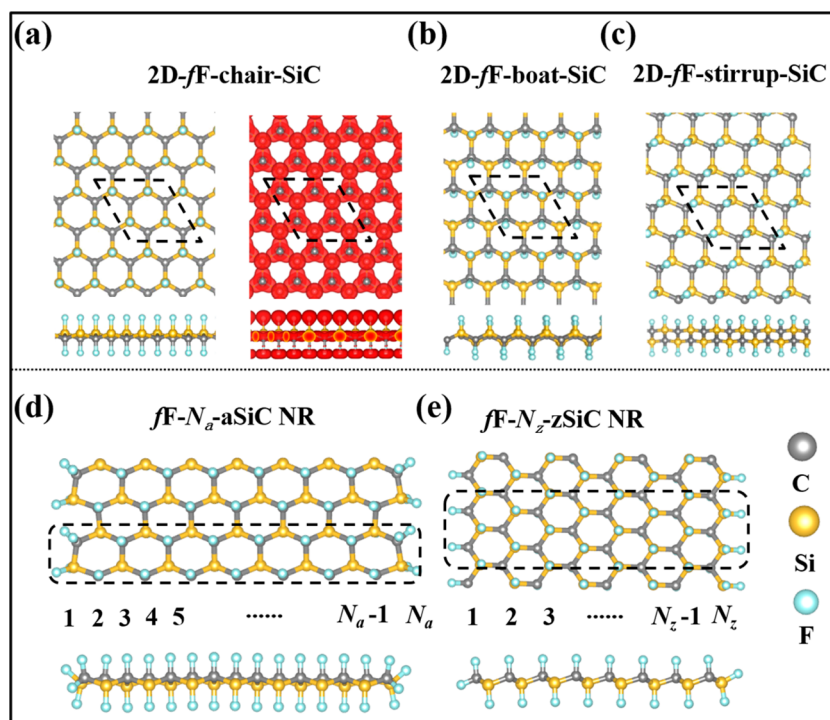
Figure 1. Top and side views of the structures of fully fluorinated (a) 2D-fF-chair-SiC (with electron localization function on the right; isosurface value 0.7 e/Å^3), (b) 2D-fF-boat-SiC, (c) 2D-fF-stirrup-SiC, (d) armchair, and (e) zigzag SiC NRs in chair configuration. The gray, yellow, and cyan balls represent C, Si, and F atoms, respectively. Unit cells are marked by dashed boxes.

gap of 2.93 eV.[30] Precise control over the F coverage enables tuning of the band gap of graphene NRs from 0 to 3.13 eV. Transitions from an NM semimetal to an NM/magnetic metal and from an NM semimetal to a magnetic/NM semiconductor can be observed.[36] Specific patterns of partially fluorinated graphene, such as nanoroads and quantum dots, also have been explored. Ferromagnetic (FM) semimetal, antiferromagnetic (AFM) semiconductor, and wide-gap semiconductor states have been achieved by tuning the orientation, width, and F coverage.[34,37]

First-principles calculations have shown that interstitial F can be used to lower the resistivity of p-type SiC.[40] Fluorination also has been applied in SiC nanostructures in order to modify the electronic and magnetic properties, in particular in nanotubes,[41,42] thin films,[43] nanowires,[44] and bilayers.[45] To our best knowledge, fluorination of 2D monolayer SiC to tailor the electronic and magnetic properties has not yet been explored. In analogy with fluorographene, it is expected that intriguing magnetic and electronic properties can be brought forth by changing the fluorination pattern and degree. We therefore perform detailed first-principles calculations and cluster expansion (CE) calculations to explore the thermodynamic stability as well as the structural, electronic, and magnetic properties of fully and partially fluorinated SiC sheets and NRs. The same method has been used before to investigate alloyed and decorated 2D systems.[46−50] The key questions to be addressed are (1) What are the ground-state atomic structures of fully and partially fluorinated 2D SiC? (2) To what extent can the electronic and magnetic properties of SiC sheets and NRs be changed by fluorination? Answering these questions will provide the understanding required for future applications in multifunctional nanodevices.

2. COMPUTATIONAL METHODS

First-principles calculations are carried out using density functional theory, as implemented in the Vienna ab initio simulation package,[51] employing the generalized gradient approximation with the Perdew−Wang functional[52] and a 360 eV cutoff for the plane wave basis set. The cutoff energy is carefully tested, see details in Figure S1 and Table S1 of the Supporting Information. Projector augmented wave[51,53] pseudopotentials are used to describe the electron−ion interactions. In all calculations, vacuum regions along nonperiodic directions (greater than 15 Å) are applied to avoid interlayer interaction. The edges of the SiC NRs are terminated by F atoms to remove dangling bonds. We employ 11 × 11 × 1 and 1 × 1 × 11 Monkhorst−Pack k-point grids in the geometry relaxations for the SiC sheets and NRs, respectively, and the total energy convergence threshold is set to 10^{-4} eV. After obtaining the equilibrium structures, 21 k-points are used between every two high symmetry k-points in the Brillouin zone to perform band structure calculations.

The stabilities of the fully and partially fluorinated SiC structures are evaluated using the formation energy per atom (E_f) defined as

$$E_f = \frac{E_{total} - n_{SiC}E_{SiC} - n_F E_F}{n}$$

Here, E_{total} is the total energy of fluorinated SiC, and E_{SiC} and E_F are the chemical potentials of the SiC dimer and F atom in the pristine SiC sheet and F$_2$ molecule, respectively. Also, n_{SiC} and n_F represent the total numbers of SiC dimers and F atoms, respectively, and $n = 2n_{SiC} + n_F$. Negative E_f implies thermodynamic stability.

To determine the ground-state structures at different concentrations, we consider the partially fluorinated SiC sheets

Table 1. Formation Energies of 2D-ƒF-SiC, ƒF-8-zSiC NR, and ƒF-15-aSiC NR in Chair, Boat, and Stirrup Configurations

|	E_f (eV/atom)		
	chair	boat	stirrup
2D-ƒF-SiC	−1.41	−1.35	−1.32
ƒF-8-zSiC NR	−1.53	−1.52	−1.53
ƒF-15-aSiC NR	−1.50	−1.48	−1.42

($SiCF_{2x}$) as a binary alloy and use the state-of-the-art CE method[54] established in alloy theory. The CE fitting of the mixing energy and the search for the thermodynamic ground state are carried out with the Alloy-Theoretic Automated Toolkit.[55] Mixing energies of the generated alloy structures are computed at the density functional theory level.

3. RESULTS AND DISCUSSION

3.1. Geometry of Fully Fluorinated Low-Dimensional SiC.
To determine the most stable configuration, we consider three conformers—chair, boat, and stirrup—of fully fluorinated SiC sheets and NRs. The relaxed structures and calculated E_f are given in Figure 1 and Table 1. Chair configurations are energetically favorable, similar to fully hydrogenated SiC NRs,[24] fluorographene, and graphene,[31] but different from hydrogenated boron nitride NRs.[56] All of the considered structures exhibit negative E_f, implying that F atoms prefer to adsorb onto the SiC sheets rather than remain in the gas phase as F_2 molecules. The chair configuration is most stable with $E_f =$ −1.41 eV/atom. A 5 ps Born−Oppenheimer molecular

dynamics (BOMD) calculation at 1000 K is performed to confirm the structural stability of this configuration using a 2 × 2 supercell. Only vibrations of atoms around their equilibrium positions are observed during the BOMD simulation. A snapshot of the atomic positions at the end of the simulation is displayed in Figure S2. The structures of the relaxed fully fluorinated SiC sheet and NRs (with both zigzag and armchair edges) are shown in Figure 1d and e. Here, the SiC NRs are labeled by the numbers of parallel armchair or zigzag chains, which define the width of the NRs. First-principles calculations reveal that all of these fully fluorinated structures have an NM ground state. In 2D fully fluorinated SiC (labeled 2D-ƒF-chair-SiC in Figure 1), the Si−C, C−F, and Si−F bond lengths are 1.818, 1.431, and 1.602 Å, respectively. The electron localization function in Figure 1a illustrates the charge distribution between the atoms and shows sp³-hybridization with significant polarization toward Si and F, as expected from the electronegativity differences of the elements. By cutting the 2D-ƒF-chair-SiC into NRs, both fully fluorinated zigzag and armchair SiC NRs (zSiC NRs and aSiC NRs) can be obtained, with the edge Si and C atoms bonded to F atoms to remove the dangling bonds (labeled ƒF-N_z-zSiC NRs and ƒF-N_a-aSiC NRs, respectively). The geometry relaxations of ƒF-N_z-zSiC NRs and ƒF-N_a-aSiC NRs of different widths (N_z = 6, 8, 10, 12, 14 and N_a = 11, 15, 17, 19, 21) result in Si−C bonds in the ranges of 1.831−1.910 Å and 1.816−1.921 Å, respectively. The Si−F and C−F bond lengths in the fully fluorinated SiC NRs are 1.587− 1.592 Å and 1.391−1.392 Å at the edge and 1.601−1.604 Å and 1.436−1.442 Å in the middle, respectively. All of the angles between Si or C atoms and their four neighbors are about 109°,
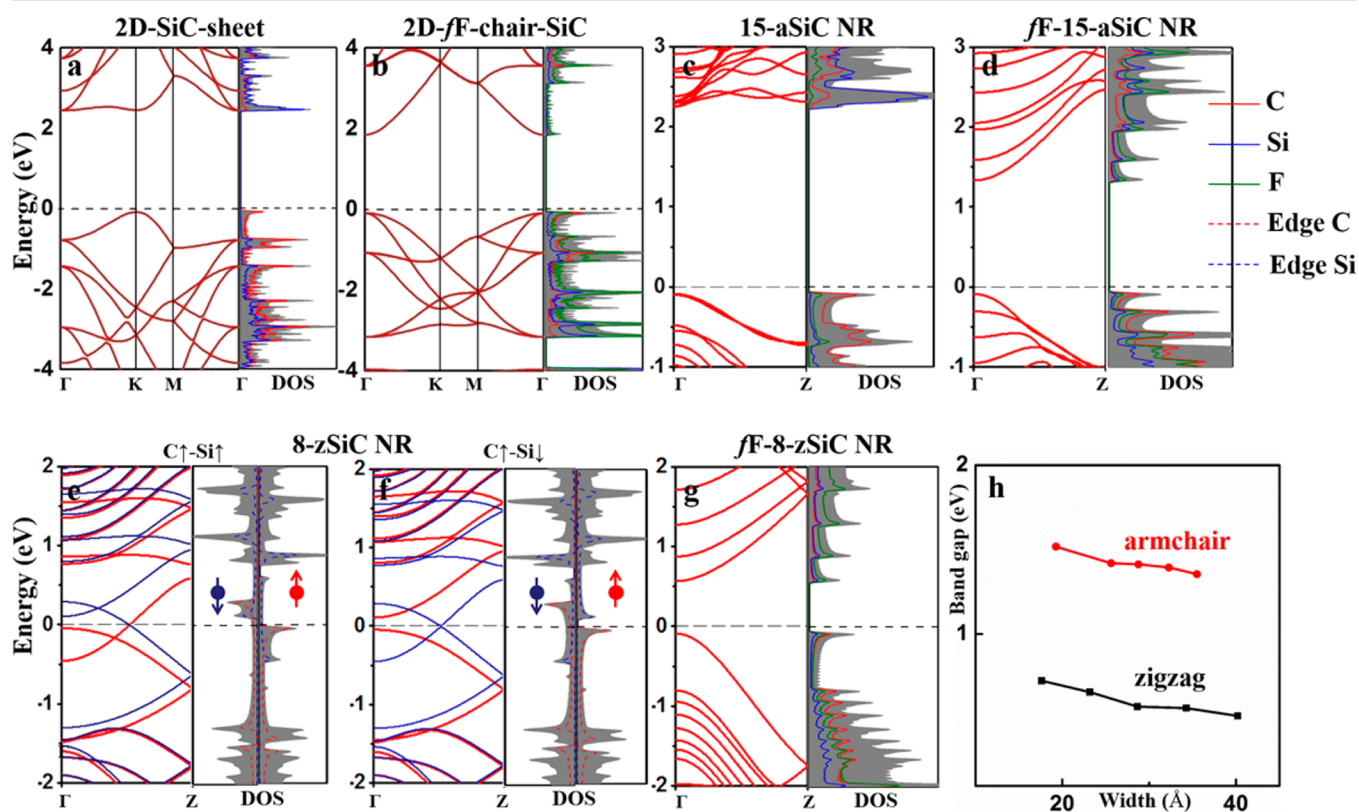
**Figure 2.** Band structures and respective DOSs for the (a) 2D-chair-SiC, (b) 2D-ƒFchair-SiC, (c) 15-aSiC NR, (d) ƒF-15-aSiC NR, (e) 8-zSiC NR in the FM state, (f) 8-zSiC NR in the AFM state, and (g) ƒF-8-zSiC NR. The Fermi level is set to zero and is indicated by black dashed lines. The total DOS is shown by gray shadows. (h) Band gaps of zigzag and armchair SiC NRs as functions of the ribbon width.
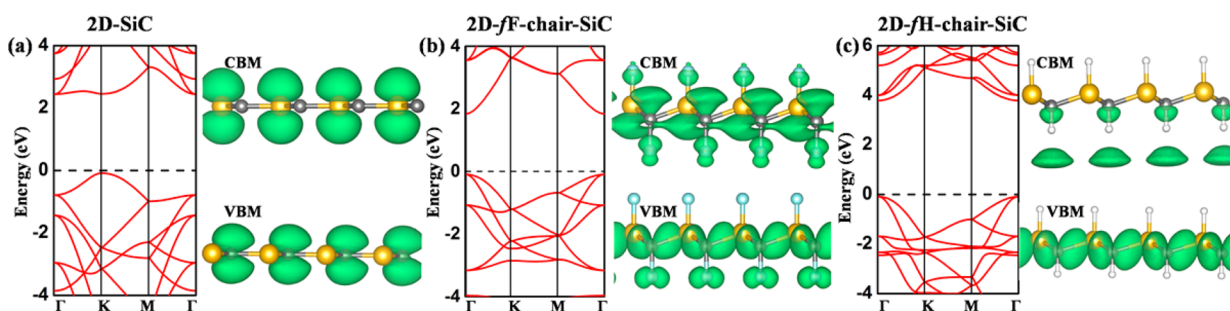
Figure 3. Band structures and corresponding partial charge densities of the VBM and CBM for the (a) pristine SiC sheet, (b) fully fluorinated SiC sheet, and (c) fully hydrogenated SiC sheet. The isosurface value is set to 2×10^{-5} e/Å^3.
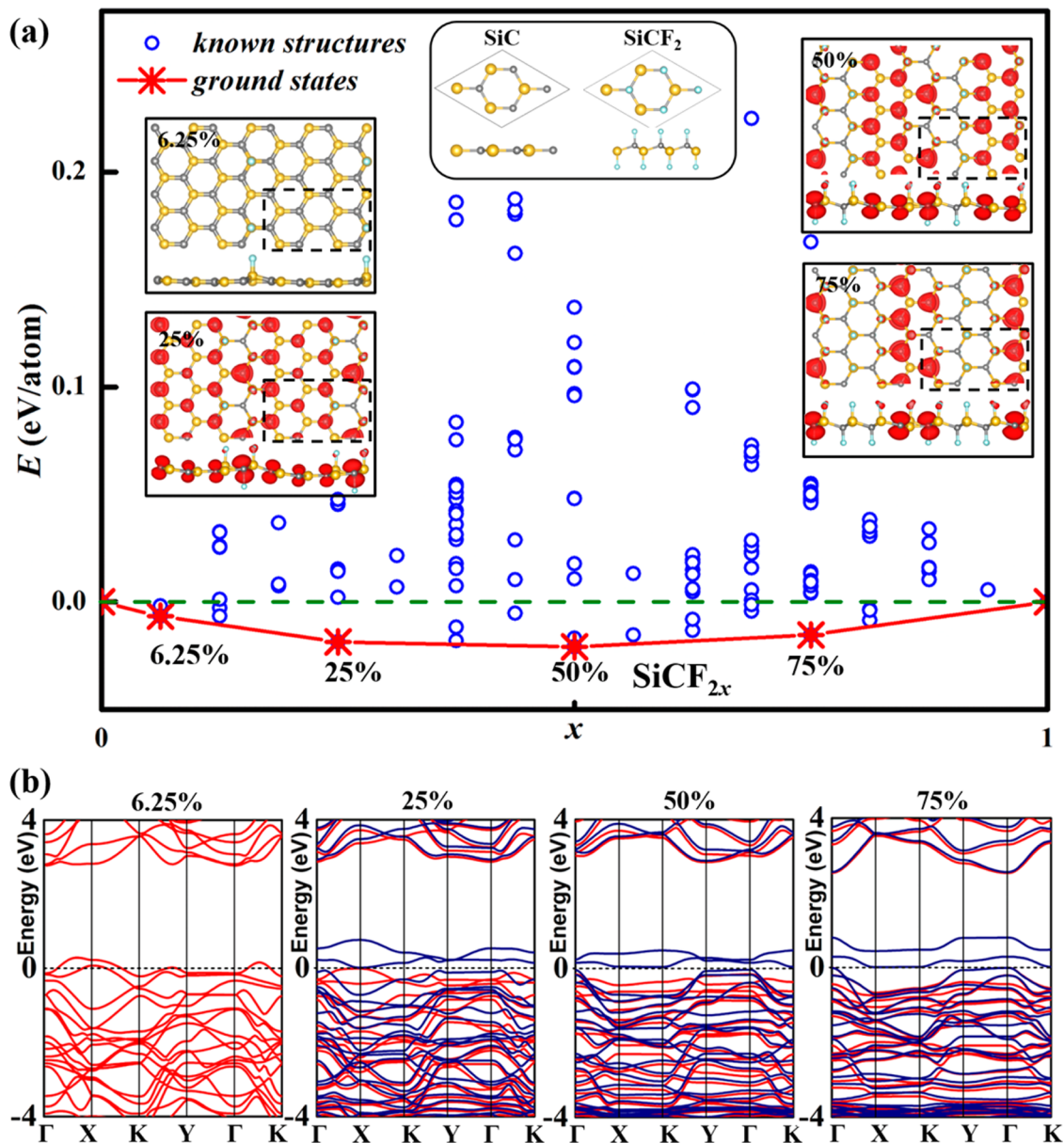
Figure 4. (a) Mixing energies of the SiCF$_{2x}$ alloy along with the corresponding CE fits as a function of x. Blue circles give the energies obtained from first-principles calculations. Red stars show the formation energies of the ground states, and the red solid line is the convex hull of the mixing energies. The insets are top and side views of the atomic configurations and spin charge densities of the ground states. The isosurface value is set to 0.004 e/Å^3, and the unit cells are marked by dashed boxes. (b) Band structures of the four ground states. Γ (0.0, 0.0, 0.0), X (0.5, 0.0, 0.0), K (0.5, 0.0, 0.5), and Y (0.0, 0.0,0.5) are high symmetry points in the first Brillouin zone. In b, the red and blue bands represent the spin-up and spin-down channels, respectively.
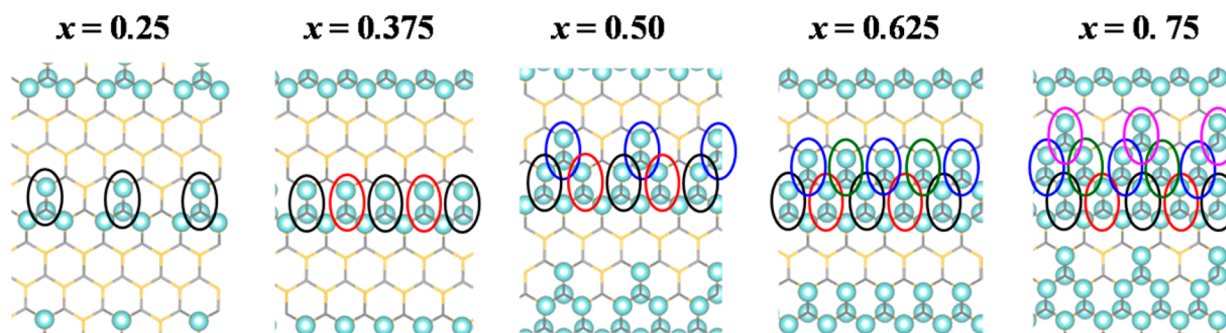
Figure 5. Structural evolution of partially fluorinated SiC sheets. The ovals of different colors designate the F dimers added to the previous structure.

indicating that the Si and C atoms in the fully fluorinated SiC NRs are also sp^3-hybridized.

3.2. Reduced Band Gap: Full Fluorination. The band structures of pristine SiC sheets and NRs are calculated by considering three reference spin configurations, namely, NM, FM, and AFM. As shown in Figure 2a, the pristine SiC sheet is an NM semiconductor with a 2.56 eV direct band gap at the K point, in agreement with a previous study.[8] By examining the calculated density of states (DOS), we find that the valence band maximum (VBM) and conduction band minimum (CBM) are mainly due to the π electrons of the C and Si atoms, respectively. After full adsorption of F atoms, the band gap decreases to 1.93 eV at the Γ point (Figure 2b). The band structures of the boat and stirrup conformers in Figure S3 (also NM semiconductors) show band gaps of 1.94 and 2.22 eV, respectively. Previously, it was reported that hydrogenation can increase the band gap of the SiC sheet from 2.53 to 3.92 eV. To reveal the band gap variation mechanism, we study the partial charge density of the VBM and CBM for pristine, fully fluorinated, and hydrogenated SiC sheets, as shown in Figure 3. For the pristine SiC sheet, the VBM and CBM (Figure 3a) are due to the π electrons of C and Si, respectively. The electrons have to overcome the barrier induced by the electronegativity difference between the C and Si atoms to be excited from the VBM to the CBM. After bonding to H atoms (Figure 3c), the sp^2 hybridization changes into sp^3. The VBM originates from the covalent C—Si electrons, while the CBM states are mainly located outside the 2D plane, where the electrons are more difficult to transfer. Because of this, the band gap of the fully hydrogenated SiC sheet is larger than that of the pristine SiC sheet. As compared to pristine and fully hydrogenated SiC sheets, the fully fluorinated structure exhibits the smallest band gap of 1.93 eV, because the VBM is due to the C—Si bonds and F atoms and the CBM is due to the corresponding antibonding states. As a result, the barrier between the VBM and CBM is smaller than in the pristine and fully hydrogenated SiC sheets. This explains why fluorination is an efficient way to decrease the band gap.

A similar situation is also observed in aSiC NRs. The band gap of the 15-aSiC NR decreases from 2.34 to 1.42 eV after full fluorination (fF-15-aSiC NR), see Figure 2c and d. The results for the pristine 8-zSiC NR show that the spin is mainly concentrated on the edge Si and C atoms, with parallel and antiparallel orientation (labeled C↑-Si↑ and C↑-Si↓ in Figure 2e and f, respectively) between the C and Si edges for the FM and AFM states. The two states are energetically almost degenerate with an energy difference of 1.0 meV. In the FM state, the pristine 8-zSiC NR exhibits a metallic nature, whereas in the AFM state, only energy levels in the spin-down

channel cross the Fermi level, indicating a half-metallic nature. The DOS shows that the edge Si and C atoms collaboratively contribute to these electronic characters. In contrast to the pristine 8-zSiC NR, the fF-8-zSiC NR is an NM semiconductor with a direct band gap of 0.67 eV at the Γ point (shown in Figure 2g). This can be attributed to the fact that the active unpaired p electrons of the edge Si and C atoms have been saturated by F atoms. To understand the origin of the metal/half-metal to semiconductor transition, we plot the DOS of the fF-8-zSiC NR in Figure 2g. Comparing with the 8-zSiC NR (Figure 2e and f), where the crossing bands are mainly due to the edge C and Si atoms, respectively, both the VBM and CBM of the fF-8-zSiC NR evenly originate from the sp^3 hybridized C, Si, and F states. The edge states govern the properties of the 8-zSiC NR but not those of the fF-8-zSiC NR. Obviously, full fluorination can lift state degeneracy, eliminate magnetism at the edge, and open a band gap in zSiC NRs.

To investigate whether the width affects the electronic properties of the fully fluorinated zSiC and aSiC NRs, detailed density functional theory calculations have been performed. The results show that all of the fluorinated SiC NRs are NM semiconductors with band structures similar to either fF-8-zSiC or fF-15-aSiC NRs. Figure 2h presents the corresponding band gaps as a function of the NR width. It is shown that the band gaps of the fF-N_z-zSiC and fF-N_a-aSiC NRs decrease monotonically from 0.72 to 0.52 eV and from 1.52 to 1.35 eV, respectively, the values being smaller than those of fully fluorinated graphene NRs[23] and hydrogenated SiC NRs[24] at similar width.

3.3. Robust Half-Metallicity: Partially Fluorinated SiC Sheet. We consider $SiCF_{2x}$ as an alloy, $x = 1$ corresponding to the fully fluorinated sheet ($SiCF_2$), with mixing energy

$$E(x) = E(SiCF_{2x}) - (1 - x)E(SiC) - xE(SiCF_2)$$

where $E(SiC)$ and $E(SiCF_2)$ are the energies per atom of SiC and $SiCF_2$ sheets, respectively. $E(SiCF_{2x})$ represents the energy per atom of the $SiCF_{2x}$ alloy. We have calculated E for 170 selected $SiCF_{2x}$ structures, containing at most 32 atoms per unit cell, by first-principles calculations. The CE Hamiltonian of $SiCF_{2x}$ is obtained by fitting to these 170 energies, and CE energies of all $SiCF_{2x}$ alloys are calculated. Four ground state structures are discovered at $x = 0.0625$, 0.25, 0.50, and 0.75, as shown in the insets of Figure 4, all in a $2 \times 2\sqrt{3}$ supercell. To establish more insights into the process of fluorination, we study the low-energy structures at various x (Figure S4) and observe that at small $x = 0.0625$ and 0.125 the F atoms only adsorb on Si atoms, as they prefer to form sp^3 rather than sp^2 hybrids. For $x = 0.25$ and larger, the F atoms bond simultaneously to Si—C dimers from different sides. It is

found from Figure 5 that F atoms are added dimer by dimer along the zigzag direction of the SiC sheet. As a result, the atomic configurations of the partially fluorinated SiC sheets are similar to the so-called nanoroad patterns of hydrogenated and fluorinated graphene.[34,57] Larger x results in narrower SiC nanoroads.

To investigate the magnetic and electronic properties of the four ground states, both spin degenerate and polarized states are considered. We find in each case an FM ground state except for $x = 0.0625$ where we have an NM ground state, because the distance between neighboring F atoms is large. In Table 2, we

Table 2. Relative Energies of SiCF$_{2x}$ in Different Magnetic States[a]

	energy (meV)			
x	NM	FM	AFM	electronic character
6.25%	0			metal
25%	138	0	43	half-metal
50%	190	0	63	half-metal
75%	176	0		half-metal

[a]The energy of the ground state is set to 0 in each case.

list the energy differences between the NM, FM, and AFM states (the energy of the ground states is set to 0 in each case). The difference from the lowest FM to the next state is at least 43 meV per unit cell, which is larger than k_BT at room temperature ($\sim$25 meV) so that the magnetic state is preserved at standard conditions. The total magnetic moments are 1.99, 2.00, and 1.99 μ_B for $x = 0.25$, 0.50, and 0.75, respectively. From the plotted spin charge densities (red contours in the insets of Figure 5a), the spin polarization is seen to be highly localized on the sp^2-C atoms in the pristine SiC part as well as in the interface, but not in the fluorinated part. The band structures of the four ground states of SiCF$_{2x}$ are shown in Figure 4b. The metallic ($x = 0.0625$) and half-metallic ($x = 0.25$, 0.50, and 0.75) states of SiCF$_{2x}$ are not similar to the semiconducting states of pristine and fully fluorinated SiC sheets. For these half-metallic structures, spin splitting can support a gap in the spin-up channel, while maintaining a metallic state in the spin-down channel. The gaps in the spin-up channel are large (2.87, 3.00, and 2.54 eV for $x = 0.25$, 0.50, and 0.75, respectively) and imply stable half-metallic properties, as required for robust spin filters. Calculated partial densities of

states (Figure S5) demonstrate that the half-metallic behavior is due to the sp^2-C atoms. The reason is that the F—Si bonding results in a reduction of the charge on neighboring C atoms and thus in partially occupied 2p$_z$ orbitals, similar to the effects of F adsorption on SiC nanotubes.[41,42]

3.4. Inactive Edges: Partially Fluorinated SiC NRs. Very often, edge states have great influence on the properties of a material. To investigate the role of edges, we calculate the band structures of partially fluorinated SiC NRs with armchair and zigzag edges. The structures are shown in Figure 6. Because the $x = 0.5$ structure possesses the lowest mixing energy, we only consider this F concentration. Dangling bonds at the edges are saturated by F atoms, and both spin degenerate and polarized states are considered. The FM energies are lower than the NM and AFM energies by more than 25 meV. We find that spin splitting is maintained in both the armchair and zigzag NRs. In the armchair NRs, the energy gaps in the spin-up and spin-down channels are 2.81 and 0.31 eV, respectively. The zigzag NR is half-metallic with a 2.95 eV band gap in the spin-up channel. From the calculated densities of states in Figure 6, we see that the states near or at the Fermi energy mainly originate from the sp^2-C atoms (red contour), same as in the 2D SiC sheet. Thus, the edge states in NRs do not affect the electronic properties of partially fluorinated SiC, implying that the system exhibits a robust and therefore useful half-metallic behavior.

4. CONCLUSION

In conclusion, our systematic density functional theory calculations show that fluorination is an efficient approach to tailoring the electronic properties of SiC sheets and NRs. Both fully and partially fluorinated SiC structures are considered. According to our results, all fully fluorinated structures are NM. Band gaps of 2D SiC sheets and armchair SiC NRs decrease from 2.56 to 1.93 eV and from 2.34 to 1.42 eV, respectively, upon fluorination. In zigzag SiC NRs, a band gap of 0.67 eV is opened. Treating the partially fluorinated SiC sheet (SiCF$_{2x}$) as an alloy, four ground state structures are obtained with the CE method. We find that the F atoms adsorb on the SiC sheet dimer by dimer along the zigzag direction, forming a nanoroad. The calculated band structures and densities of states demonstrate that a robust half-metallic behavior, governed by the sp^2-C atoms, can be achieved at $x = 0.25$, 0.5, and 0.75. The edge states do not affect the electronic properties significantly. Spin splitting and large energy gap differences between the
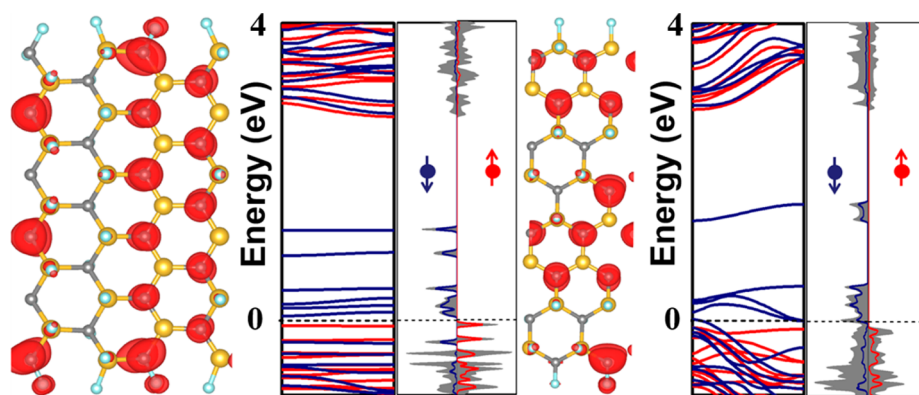
Figure 6. Top views of the atomic configurations, spin charge densities, band structures, and DOSs of armchair (left) and zigzag (right) half-fluorinated SiC NRs. Red and blue colors represent the spin-up and spin-down channels, respectively. Gray shadows show the total DOS, and the lines show the partial DOS of the sp^2-C atoms.

spin-up and spin-down channels are ideal for spin filters. Our findings can aid applications of 2D SiC materials in nano-electronic devices.

■ ASSOCIATED CONTENT

Ⓢ Supporting Information

The Supporting Information is available free of charge on the ACS Publications website at DOI: 10.1021/acs.jpcc.6b01706.

> Bond lengths, band stuctures, structural transition with increasing F concentration, DOSs of the partially fluorinated SiC sheet
> (PDF)

■ AUTHOR INFORMATION

Corresponding Authors

*E-mail: Udo.Schwingenschlogl@kaust.edu.sa.
*E-mail: huangxr@jlu.edu.cn.

Notes

The authors declare no competing financial interest.

■ ACKNOWLEDGMENTS

■ REFERENCES

(1) Novoselov, K. S.; Geim, A. K.; Morozov, S. V.; Jiang, D.; Zhang, Y.; Dubonos, S. V.; Grigorieva, I. V.; Firsov, A. A. Electric Field Effect in Atomically Thin Carbon Films. *Science* **2004**, *306*, 666−669.

(2) Novoselov, K. S.; Jiang, D.; Schedin, F.; Booth, T. J.; Khotkevich, V. V.; Morozov, S. V.; Geim, A. K. Two-Dimensional Atomic Crystals. *Proc. Natl. Acad. Sci. U. S. A.* **2005**, *102*, 10451−10453.

(3) Allen, M. J.; Tung, V. C.; Kaner, R. B. Honeycomb Carbon: A Review of Graphene. *Chem. Rev.* **2010**, *110*, 132−145.

(4) Katsnelson, M. I.; Novoselov, K. S.; Geim, A. K. Chiral Tunnelling and the Klein Paradox in Graphene. *Nat. Phys.* **2006**, *2*, 620−625.

(5) Zhang, Y. B.; Tan, Y. W.; Stormer, H. L.; Kim, P. Experimental Observation of the Quantum Hall Effect and Berry's Phase in Graphene. *Nature* **2005**, *438*, 201−204.

(6) Lee, C.; Wei, X. D.; Kysar, J. W.; Hone, J. Measurement of the Elastic Properties and Intrinsic Strength of Monolayer Graphene. *Science* **2008**, *321*, 385−388.

(7) Coleman, J. N.; Lotya, M.; O'Neill, A.; Bergin, S. D.; King, P. J.; Khan, U.; Young, K.; Gaucher, A.; De, S.; Smith, R. J.; Shvets, I. V.; Arora, S. K.; Stanton, G.; Kim, H. Y.; Lee, K.; Kim, G. T.; Duesberg, G. S.; Hallam, T.; Boland, J. J.; Wang, J. J.; Donegan, J. F.; Grunlan, J. C.; Moriarty, G.; Shmeliov, A.; Nicholls, R. J.; Perkins, J. M.; Grieveson, E. M.; Theuwissen, K.; McComb, D. W.; Nellist, P. D.; Nicolosi, V. Two-Dimensional Nanosheets Produced by Liquid Exfoliation of Layered Materials. *Science* **2011**, *331*, 568−571.

(8) Sahin, H.; Cahangirov, S.; Topsakal, M.; Bekaroglu, E.; Akturk, E.; Senger, R. T.; Ciraci, S. Monolayer Honeycomb Structures of Group-IV Elements and III-V Binary Compounds: First-Principles Calculations. *Phys. Rev. B: Condens. Matter Mater. Phys.* **2009**, *80*, 155453.

(9) Lin, S. S. Light-Emitting Two-Dimensional Ultrathin Silicon Carbide. *J. Phys. Chem. C* **2012**, *116*, 3951−3955.

(10) Li, H.; Cao, C. B.; Hao, H. W.; Qiu, H. L.; Xu, Y. J.; Zhu, H. S. Self-Assembled One-Dimensional Carbon Nitride Architectures. *Diamond Relat. Mater.* **2006**, *15*, 1593−1600.

(11) Chen, S. J.; Liu, Y. C.; Shao, C. L.; Mu, R.; Lu, Y. M.; Zhang, J. Y.; Shen, D. Z.; Fan, X. W. Structural and Optical Properties of Uniform ZnO Nanosheets. *Adv. Mater.* **2005**, *17*, 586−590.

(12) Zeng, Z. Y.; Yin, Z. Y.; Huang, X.; Li, H.; He, Q. Y.; Lu, G.; Boey, F.; Zhang, H. Single-Layer Semiconducting Nanosheets: High-Yield Preparation and Device Fabrication. *Angew. Chem., Int. Ed.* **2011**, *50*, 11093−11097.

(13) Wu, R. B.; Wu, L. L.; Yang, G. Y.; Pan, Y.; Chen, J. J.; Zhai, R.; Lin, J. Fabrication and Photoluminescence of Bicrystalline Sic Nanobelts. *J. Phys. D: Appl. Phys.* **2007**, *40*, 3697−3701.

(14) Gao, F. M.; Yang, W. Y.; Wang, H. T.; Fan, Y.; Xie, Z. P.; An, L. A. Controlled Al-Doped Single-Crystalline 6H-SiC Nanowires. *Cryst. Growth Des.* **2008**, *8*, 1461−1464.

(15) Zhang, H. A.; Ding, W. Q.; He, K.; Li, M. Synthesis and Characterization of Crystalline Silicon Carbide Nanoribbons. *Nanoscale Res. Lett.* **2010**, *5*, 1264−1271.

(16) Bekaroglu, E.; Topsakal, M.; Cahangirov, S.; Ciraci, S. First-Principles Study of Defects and Adatoms in Silicon Carbide Honeycomb Structures. *Phys. Rev. B: Condens. Matter Mater. Phys.* **2010**, *81*, 075433.

(17) Zhang, J. M.; Zheng, F. L.; Zhang, Y.; Ji, V. First-Principles Study on Electronic Properties of SiC Nanoribbon. *J. Mater. Sci.* **2010**, *45*, 3259−3265.

(18) Lou, P.; Lee, J. Y. Spin Controlling in Narrow Zigzag Silicon Carbon Nanoribbons by Carrier Doping. *J. Phys. Chem. C* **2010**, *114*, 10947−10951.

(19) He, X. J.; He, T.; Wang, Z. H.; Zhao, M. W. Neutral Vacancy-Defect-Induced Magnetism in SiC Monolayer. *Phys. E* **2010**, *42*, 2451−2454.

(20) Guan, J.; Yu, G. T.; Ding, X. L.; Chen, W.; Shi, Z. M.; Huang, X. R.; Sun, C. C. The Effects of the Formation of Stone-Wales Defects on the Electronic and Magnetic Properties of Silicon Carbide Nanoribbons: A First-Principles Investigation. *ChemPhysChem* **2013**, *14*, 2841−2852.

(21) Lou, P.; Lee, J. Y. Electrical Control of Magnetization in Narrow Zigzag Silicon Carbon Nanoribbons. *J. Phys. Chem. C* **2009**, *113*, 21213−21217.

(22) Lou, P. Nonmagnetic Impurity Chemistry Substitution Effects in Zigzag Silicon Carbide Nanoribbons. *Phys. Status Solidi B* **2013**, *250*, 1265−1277.

(23) Tang, S. B.; Zhang, S. Y. Structural and Electronic Properties of Hybrid Fluorographene-Graphene Nanoribbons: Insight from First-Principles Calculations. *J. Phys. Chem. C* **2011**, *115*, 16644−16651.

(24) Guan, J.; Chen, W.; Zhao, X. J.; Yu, G. T.; Huang, X. R.; Sun, C. C. Successive Hydrogenation Starting from the Edge(S): An Effective Approach to Fine-Tune the Electronic and Magnetic Behaviors of SiC Nanoribbons. *J. Mater. Chem.* **2012**, *22*, 24166−24172.

(25) Ding, X. L.; Yu, G. T.; Huang, X. R.; Chen, W. The Donor/Acceptor Edge-Modification: An Effective Strategy to Modulate the Electronic and Magnetic Behaviors of Zigzag Silicon Carbon Nanoribbons. *Phys. Chem. Chem. Phys.* **2013**, *15*, 18039−18047.

(26) Lou, P. Effects of Edge Hydrogenation in Zigzag Silicon Carbide Nanoribbons: Stability, Electronic and Magnetic Properties, as Well as Spin Transport Property. *J. Mater. Chem. C* **2013**, *1*, 2996−3003.

(27) Chen, W.; Zhang, H.; Ding, X. L.; Yu, G. T.; Liu, D.; Huang, X. R. Dihalogen Edge-Modification: An Effective Approach to Realize the Half-Metallicity and Metallicity in Zigzag Silicon Carbon Nanoribbons. *J. Mater. Chem. C* **2014**, *2*, 7836−7850.

(28) Zhang, Z. H.; Guo, W. L. Tunable Ferromagnetic Spin Ordering in Boron Nitride Nanotubes with Topological Fluorine Adsorption. *J. Am. Chem. Soc.* **2009**, *131*, 6874−6879.

(29) Nair, R. R.; Ren, W. C.; Jalil, R.; Riaz, I.; Kravets, V. G.; Britnell, L.; Blake, P.; Schedin, F.; Mayorov, A. S.; Yuan, S. J.; Katsnelson, M. I.; Cheng, H. M.; Strupinski, W.; Bulusheva, L. G.; Okotrub, A. V.;

Grigorieva, I. V.; Grigorenko, A. N.; Novoselov, K. S.; Geim, A. K. Fluorographene: A Two-Dimensional Counterpart of Teflon. *Small* **2010**, *6*, 2877−2884.

(30) Robinson, J. T.; Burgess, J. S.; Junkermeier, C. E.; Badescu, S. C.; Reinecke, T. L.; Perkins, F. K.; Zalalutdniov, M. K.; Baldwin, J. W.; Culbertson, J. C.; Sheehan, P. E.; Snow, E. S. Properties of Fluorinated Graphene Films. *Nano Lett.* **2010**, *10*, 3001−3005.

(31) Leenaerts, O.; Peelaers, H.; Hernandez-Nieves, A. D.; Partoens, B.; Peeters, F. M. First-Principles Investigation of Graphene Fluoride and Graphane. *Phys. Rev. B: Condens. Matter Mater. Phys.* **2010**, *82*, 195436.

(32) Withers, F.; Dubois, M.; Savchenko, A. K. Electron Properties of Fluorinated Single-Layer Graphene Transistors. *Phys. Rev. B: Condens. Matter Mater. Phys.* **2010**, *82*, 073403.

(33) Zhou, J.; Wang, Q.; Sun, Q.; Jena, P. Electronic and Magnetic Properties of a BN Sheet Decorated with Hydrogen and Fluorine. *Phys. Rev. B: Condens. Matter Mater. Phys.* **2010**, *81*, 085442.

(34) Ribas, M. A.; Singh, A. K.; Sorokin, P. B.; Yakobson, B. I. Patterning Nanoroads and Quantum Dots on Fluorinated Graphene. *Nano Res.* **2011**, *4*, 143−152.

(35) Bhattacharya, A.; Bhattacharya, S.; Das, G. P. Strain-Induced Band-Gap Deformation of H/F Passivated Graphene and H-BN Sheet. *Phys. Rev. B: Condens. Matter Mater. Phys.* **2011**, *84*, 075454.

(36) Liu, H. Y.; Hou, Z. F.; Hu, C. H.; Yang, Y.; Zhu, Z. Z. Electronic and Magnetic Properties of Fluorinated Graphene with Different Coverage of Fluorine. *J. Phys. Chem. C* **2012**, *116*, 18193−18201.

(37) Shi, H. L.; Pan, H.; Zhang, Y. W.; Yakobson, B. I. Electronic and Magnetic Properties of Graphene/Fluorographene Superlattices. *J. Phys. Chem. C* **2012**, *116*, 18278−18283.

(38) Tang, S. B.; Yu, J. P.; Liu, L. X. Tunable Doping and Band Gap of Graphene on Functionalized Hexagonal Boron Nitride with Hydrogen and Fluorine. *Phys. Chem. Chem. Phys.* **2013**, *15*, 5067−5077.

(39) Gao, D. Q.; Shi, S. P.; Tao, K.; Xia, B. R.; Xue, D. S. Tunable Ferromagnetic Ordering in MoS$_2$ Nanosheets with Fluorine Adsorption. *Nanoscale* **2015**, *7*, 4211−4216.

(40) Miyata, M.; Hattori, S.; Hayafuji, Y. Electronic Structures of 4H-SiC with Group I and VII Elements: First-Principles Study of Possible P-Type Doping. *Jpn. J. Appl. Phys.* **2009**, *48*, 041301.

(41) Zhao, J. X.; Ding, Y. H.; Cai, Q. H.; Wang, X. G.; Wang, X. Z. Theoretical Studies of the Magnetism of the First-Row Adatom on the Silicon Carbide (SiC) Nanotube. *J. Phys. Chem. C* **2010**, *114*, 3825−3829.

(42) Wang, X.; Liew, K. M. Density Functional Study of Fluorinated Single-Walled Silicon Carbide Nanotubes. *J. Phys. Chem. C* **2012**, *116*, 1702−1708.

(43) Batisse, N.; Guérin, K.; Dubois, M.; Hamwi, A.; Spinelle, L.; Tomasella, E. Fluorination of Silicon Carbide Thin Films Using Pure F$_2$ Gas or XeF$_2$. *Thin Solid Films* **2010**, *518*, 6746−6751.

(44) Miranda, A.; Cruz-Irisson, M.; Perez, L. A. Controlling Stability and Electronic Properties of Small-Diameter SiC Nanowires by Fluorination. *Int. J. Nanotechnol.* **2015**, *12*, 218−225.

(45) Gao, B. L.; Wang, B. L.; Xu, Q. Q.; Xiong, S. J. Ferromagnetic and Antiferromagnetic Properties of the Fluorinated Bilayer SiC Sheets. *Phys. E* **2011**, *43*, 1394−1397.

(46) Huang, B.; Xiang, H.; Wei, S.-H. Chemical Functionalization of Silicene: Spontaneous Structural Transition and Exotic Electronic Properties. *Phys. Rev. Lett.* **2013**, *111*, 145502.

(47) Huang, B.; Xiang, H.; Xu, Q.; Wei, S.-H. Overcoming the Phase Inhomogeneity in Chemically Functionalized Graphene: The Case of Graphene Oxides. *Phys. Rev. Lett.* **2013**, *110*, 085501.

(48) Kutana, A.; Penev, E. S.; Yakobson, B. I. Engineering Electronic Properties of Layered Transition-Metal Dichalcogenide Compounds through Alloying. *Nanoscale* **2014**, *6*, 5820−5825.

(49) Shi, Z.; Zhang, Z.; Kutana, A.; Yakobson, B. I. Predicting Two-Dimensional Silicon Carbide Monolayers. *ACS Nano* **2015**, *9*, 9802−9809.

(50) Shi, Z. M.; Kutana, A.; Yakobson, B. I. How Much N-Doping Can Graphene Sustain? *J. Phys. Chem. Lett.* **2015**, *6*, 106−112.

(51) Kresse, G.; Joubert, D. From Ultrasoft Pseudopotentials to the Projector Augmented-Wave Method. *Phys. Rev. B: Condens. Matter Mater. Phys.* **1999**, *59*, 1758−1775.

(52) Perdew, J. P.; Chevary, J. A.; Vosko, S. H.; Jackson, K. A.; Pederson, M. R.; Singh, D. J.; Fiolhais, C. Atoms, Molecules, Solids, and Surfaces - Applications of the Generalized Gradient Approximation for Exchange and Correlation (Vol 46, Pg 6671, 1992). *Phys. Rev. B: Condens. Matter Mater. Phys.* **1993**, *48*, 4978−4978.

(53) Blochl, P. E. Projector Augmented-Wave Method. *Phys. Rev. B: Condens. Matter Mater. Phys.* **1994**, *50*, 17953−17979.

(54) Sanchez, J. M.; Ducastelle, F.; Gratias, D. Generalized Cluster Description of Multicomponent Systems. *Phys. A* **1984**, *128*, 334−350.

(55) van de Walle, A.; Asta, M.; Ceder, G. The Alloy Theoretic Automated Toolkit: A User Guide. *CALPHAD: Comput. Coupling Phase Diagrams Thermochem.* **2002**, *26*, 539−553.

(56) Shi, Z. M.; Zhao, X. G.; Huang, X. R. First Principles Investigation on the Stability, Magnetic and Electronic Properties of the Fully and Partially Hydrogenated BN Nanoribbons in Different Conformers. *J. Mater. Chem. C* **2013**, *1*, 6890−6898.

(57) Singh, A. K.; Yakobson, B. I. Electronics and Magnetism of Patterned Graphene Nanoroads. *Nano Lett.* **2009**, *9*, 1540−1543.